Catalysis Today 259 (2015) 165–176

Contents lists available at ScienceDirect

Catalysis Today

journal homepage: www.elsevier.com/locate/cattod

Development of an active, selective and durable water-gas shift catalyst for use in membrane reactors

E.A. Lombardo*, C. Cornaglia, J. Múnera

Instituto de Investigaciones en Catálisis y Petroquímica, INCAPE (FIQ, UNL-CONICET), Santiago del Estero 2829 Santa Fe, (S3006BMF), Argentina

ARTICLE INFO

Article history:
Received 9 March 2015
Received in revised form 19 June 2015
Accepted 23 June 2015
Available online 1 September 2015

Keywords:
Pt
combined oxides
H_2 production
durability tests
Rh/La_2O_3 deactivation

ABSTRACT

$Rh(0.6\%)/La_2O_3$ and $Rh(0.6\%)/La_2O_3(27\,wt\%)\cdot SiO_2$ **were** assayed for the WGS reaction at 673 K and 1 atm. They were both more active than industrial Cr-Fe based catalysts. $Rh(0.6\%)/La_2O_3$ was the most active but it progressively deactivated. To investigate its deactivation and the stability of the $Rh(0.6\%)/La_2O_3(27\,wt\%)\cdot SiO_2$, the WGS reaction was carried out in a DRIFTS cell in operando mode. The deactivation of the former was due to the strong adsorption of intermediate oxygenates. Another disadvantage of the Rh formulations was their methanation activity. Therefore, a series of formulations containing 0.1 wt% through 1.2 wt% Pt supported on $La_2O_3(27\,wt\%)\cdot SiO_2$ were synthesized and catalytically evaluated in a fixed-bed reactor. The activity, methane formation and stability were carefully checked. The fresh and used catalysts were characterized through a battery of techniques including XRD, LRS and XPS. The Pt(0.1 wt%) formulation resulted the most active one per gram of platinum and negligible methanation occurred. It maintained the activity and selectivity after 155 h on stream. This catalyst was tested in a Pd-Ag membrane reactor to produce ultrapure H_2 (<10 ppm of CO) that can be used to feed a low temperature PEM fuel cell. Comparing our results with those already published, it is concluded that our system is one of the best ones reported so far.

© 2015 Elsevier B.V. All rights reserved.

1. Introduction

Our group at INCAPE has been studying the performance of noble metals supported over La containing oxides for roughly 15 years for several reactions such as dry reforming [1,2], combined reforming [3] and the water gas shift reaction [4–8]. We published the first article on WGSR in 2011 [4]. In this revision of our work, we concentrate upon the latter reaction with a view to pointing out the most promising formulation to be employed in membrane reactors to produce ultrapure hydrogen (<10 ppm CO) for use in PEM fuel cells.

The most often tried catalysts in membrane reactors are the recent versions of the Fe-Cr type containing up to date promoters. These formulations are very selective and stable under steady – state operation, which applies to the industrial purification of H_2 to be used in ammonia synthesis and other petrochemical applications. However, they are not well suited for those applications where the operation is often turned on and off as it occurs in fuel processors [9]. Farrauto and co-workers have demonstrated that the stability of WGS catalysts is strongly affected by frequent stop-start operations [10]. Cr toxicity is another troubling factor. These are the main driving forces behind the numerous research efforts to find alternative formulations for the WGSR.

Authoritative reviews have already been published about the catalytic reaction itself [11]. Accordingly, in this review we will specifically refer to those publications addressing the development of catalysts for use in a portable hydrogen generator and similar applications to produce ultrapure H_2. Kondarides and co-workers studied a good number of doped CeO_2 supports over which Pt was deposited [12]. The main conclusion they reached is that the effectiveness of the support increases with the reducibility of the main oxide and the decreasing crystallite size of the doping oxide.

$Pt/Ce_xZr_{1-x}O_2$ was also explored for WGSR. Formulations going from pure CeO_2 to pure ZrO_2 have been studied as Pt supports for the WGS reaction. Vignatti et al. [13] systematically investigated the effect of Zr substitution in CeO_2 on the catalytic behavior. They observed that the formulations richer in cerium were the most active ones. They concluded that this was due to a weaker chemisorption of the formate intermediates on cerium rich solids.

We have successfully used the $Rh(0.6)/La_2O_3$ and $Rh(0.6)/La_2O_3(27)\cdot SiO_2$ for the dry [2,14] and the combined reforming [3] of methane. So we decided to start our WGS studies with these formulations.

* Corresponding author. Tel.: +54 342 4536861; fax: +54 342 4536861.
E-mail address: nfisico@fiq.unl.edu.ar (E.A. Lombardo).

http://dx.doi.org/10.1016/j.cattod.2015.06.015
0920-5861/© 2015 Elsevier B.V. All rights reserved.

2. Experimental

2.1. Catalysts preparation

The Rh(0.6 wt %)/La_2O_3 catalyst was prepared by the conventional wet impregnation of La_2O_3 (Alfa Aesar, 99.99%) using $RhCl_3$ $3H_2O$ (Alfa Aesar, 99.99%). The resulting suspension was then heated at 353 K to evaporate the water and the solid material was dried in an oven at 383 K overnight.

The La_2O_3·SiO_2 support was prepared by the incipient wetness impregnation of SiO_2 with lanthanum nitrate (Anedra), calcined at 873 K. After calcination, the load of lanthanum given as La_2O_3 was 27 wt%. The SiO_2 (Aerosil 300) employed in the solid preparation was previously calcined at 1173 K.

The Pt and Rh supported on this oxide were prepared by incipient wetness impregnation using $Pt(NH_3)_4.Cl_2.H_2O$ (Strem Chemicals, Inc., 99.95%-Pt) and $RhCl_3.6H_2O$ (Alfa Aesar, 99.99%) as precursors. The samples were kept at room temperature for 4 h and then dried at 343 K overnight.

2.2. Catalysts characterization

The fresh-reduced and used (after exposure to WGSR conditions) catalysts were analyzed by X-Ray Diffraction (XRD) using an XD-D1 Shimadzu instrument and Cu Kα radiation at 30 kV and 40 mA. The scanning rate was 1.0°/min for values between $2\theta = 10°$ and 60°. BET surface areas (S_g) were measured by N_2 physisorption at its boiling point in a Micromeritics Accusorb 2100 E sorptometer.

The Raman spectra of fresh and used solids were recorded using a LabRam spectrometer (Horiba-Jobin-Yvon) coupled to an Olympus confocal microscope (a 100X objective lens was used for simultaneous illumination and collection), equipped with a CCD detector cooled to about 200 K using the Peltier effect. The excitation wavelength was in all cases 532 nm (Spectra Physics diode pump solid state laser). The laser power was set at 30 mW.

The XPS measurements were carried out using a multitechnique system (SPECS) equipped with a dual Mg/Al X-ray source and a hemispherical PHOIBOS 150 analyzer operating in the fixed analyzer transmission (FAT) mode. The spectra were obtained with pass energy of 30 eV; the Mg Ka X-ray source was operated at 200 W and 12 kV. The working pressure in the analyzing chamber was less than 6×10^{-7} Pa. The XPS analyses were performed on the solids after treatment with hydrogen at 673 K carried out in the reaction chamber of the spectrometer.

Operando DRIFTS (Diffuse Reflectance Infrared Fourier-Transform Spectroscopy) was performed with a Bruker Equinox 55 infrared spectrometer equipped with an air cooled MIR source with KBr optics and an MCT detector. Spectra were obtained by collecting 200 scans with a resolution of 4 cm^{-1}. The catalysts were placed without packing or dilution inside a cell with controlled temperature and environment (Spectra-Tech 0030-102) equipped with ZnSe windows.

2.3. Catalytic measurements

2.3.1. Conventional fixed-bed reactor

Catalytic measurements were conducted in a conventional flow system isothermally operated at atmospheric pressure. The tubular quartz reactor had an inner diameter of 9.5 mm. The feed stream gas mixture was made up of CO, H_2O and Ar. CO and Ar flow rates were controlled using MKS mass flow controllers, while the steam was generated in a preheater fed with water from a syringe pump (Apema S.R.L.) at the desired flow rate. The reaction temperature was controlled through a thermocouple placed inside the catalyst bed. The catalysts were heated in Ar at 673 K at a rate of 1.5 K min^{-1}. Afterwards, they were reduced in flowing H_2 at the same temperature for 2 h. The gases leaving the reactor flowed through an ice-cooled trap and a tube packed with silica gel to remove water before the gas chromatographic analysis. The feed and product streams were analyzed with a Shimadzu 9A thermal conductivity detector (TCD) gas chromatograph equipped with a Hayezep D column for the complete separation of the gaseous components.

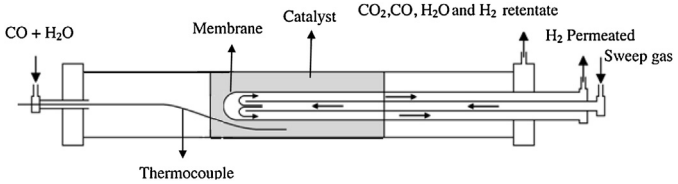

Fig. 1. Membrane reactor scheme.

2.3.2. Membrane reactor

The reaction was carried out using a double tubular membrane reactor operated isothermally. The membrane reactor was built using a commercial dense Pd-Ag (77–23%) alloy (50 μm thick and external diameter of 3.2 mm) provided by REB Research and Consulting, with one end closed and an inner tube to feed sweep gas, i.e. Ar. The outer tube was made of commercial non-porous quartz. The catalyst (150 mg), diluted with quartz chips (5000 mg), to cover a membrane area of 7×10^{-4} m^2 was packed in the annular region (Fig. 1). The membrane was 100% selective, so only hydrogen was detected on the permeate side, even after several hundred hours on stream under reaction conditions. This was determined using a mass spectrometer with a detection limit of impurities of 1 ppm.

In blank studies (Only silica chips in the lumen of the MR) we found no catalytic activity of the membrane.

3. Results and discussion

3.1. Rh supported over different La- containing oxides

Activity and stability. Two different La- containing formulations (Rh(0.6)/La_2O_3(27)·SiO_2 and Rh(0.6)/La_2O_3) were studied under WGS conditions, at 673 K and H_2O:CO = 3:1, in differential mode (X_{CO} < 10%) and in the absence of mass transport limitations. Table 1 shows the initial activities of these catalysts. The activity of a promoted Cr-Fe commercial formulation was also measured for comparison purposes. Note that the solids containing Rh were more active than the traditional formulation.

Fig. 2 shows that the CO rate was constant for at least 50 h for the Rh(0.6)/La_2O_3(27)·SiO_2 catalyst, while Rh(0.6)/La_2O_3 suffered a progressive deactivation.

Since the initial reaction rate for the La_2O_3 supported catalyst was ca. 60% higher than the La_2O_3·SiO_2 based catalyst (Table 1 and Fig. 2), this was a driving force to investigate the nature of the deactivation process of the Rh(0.6)/La_2O_3 formulation that could lead to the design of better catalysts for the WGS reaction.

Catalysts characterization. The catalysts fresh-reduced and used under reaction condition were characterized by XRD, LRS, FTIR and XPS. However, with the use of these techniques it was not possible

Table 1
Activity measurement at 673 K of supported Rh and Fe-Cr catalysts.

Catalyst	Dispersion	Initial rate ($\times 10^4$ mol g^{-1} s^{-1})[a]	Ref
Rh(0.6)/La_2O_3	14	2.65	[5]
Rh(0.6)/La_2O_3(27)·SiO_2	79	1.65	[5]
Promoted Fe-Cr	–	0.52	[7]

[a] Feed composition: 9% CO, 27% H_2O and 64% Ar.

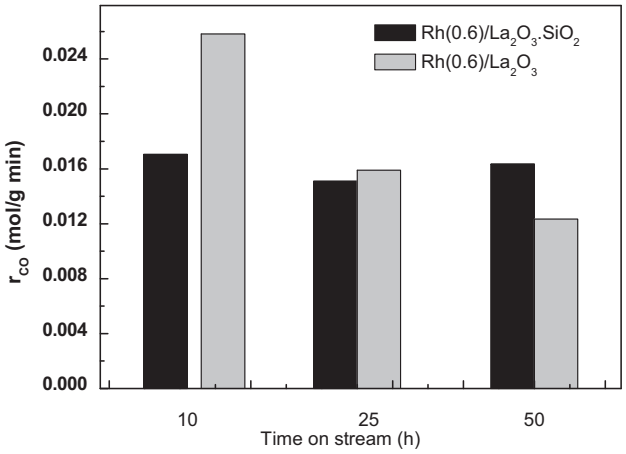

Fig. 2. Stability tests for $Rh(0.6)/La_2O_3(27)\cdot SiO_2$ and $Rh(0.6)/La_2O_3$ at 673 K, 1 atm and $H_2O/CO = 3$.

to determine the cause of catalyst deactivation supported on La_2O_3 (For more details see [4,5])

The next step is to further explore the catalytic stability of the lanthanum containing formulations trying to ascertain the origin and possible cure of the deactivation of the $Rh(0.6)/La_2O_3$.

3.2. Ascertaining the nature of the deactivation process

Different fixed-bed reactor measurements and "operando" DRIFT experiments were performed. Note that the use of the latter technique is particularly important because the formation of the different species adsorbed on the surface of the catalysts can be studied in real time, thus making it possible to investigate the influence of these adsorbed species on the deactivation process.

Through qualitative or semi quantitative methods, several authors have reported that the deactivation causes of WGS formulations may be broadly due to: (i) loss of metal surface area (sintering) [16], (ii) chemical transformation of support materials and/or catalysts [17], (iii) carbon deposition [18], (iv) strong adsorption of carbonate/formate species [10,19].

3.2.1. Drifts operando study over both catalytic systems under WGS conditions

DRIFT spectra of the $Rh(0.6)/La_2O_3(27)\cdot SiO_2$and $Rh(0.6)/La_2O_3$ catalysts obtained during exposure to a reacting mixture (1.1% H_2O, 1.1% CO, 98.8% He) at 673 K, are shown in Fig. 3. The evolution of the mass spectrometer signals during the WGS reaction was also recorded (not shown) [5].

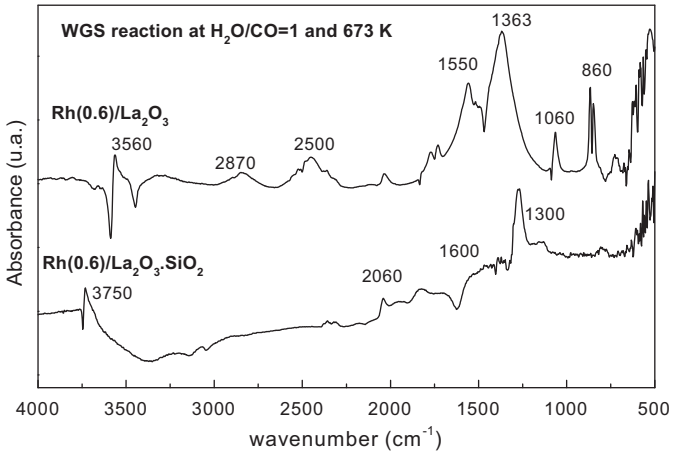

Fig. 3. DRIFT spectra obtained during the WGS reaction with 1.1% H_2O + 1.1%CO + 98.8%He at 673K.

Fig. 3 shows an absorption band at 3750 cm^{-1}, most likely associated with the existence of isolated silanol groups [20]. The shoulder of this band at a lower wavenumber is likely due to hydrogen bonded adjacent hydroxyls.

The band at 2060 cm^{-1} is assigned to CO linearly adsorbed on Rh. At 673 K, this band remains unchanged even after exposure to He during 15 min at the same temperature (not shown).

For the $Rh(0.6)/La_2O_3(27)\cdot SiO_2$ catalyst (Fig. 3) and the La-Si support (not shown), a well-defined band at 1300 cm^{-1} is observed. This signal could not be assigned to a particular feature of these solids. Clearly, this band does not belong to species formed during the WGS reaction. The presence of a negative band at 1600 cm^{-1} corresponds to adsorbed water present in the reference spectrum. It decreases with increasing temperature.

The DRIFT spectrum of the $Rh(0.6)/La_2O_3$ catalyst (Fig. 3) shows bands at 720, 842, 860, 1060, 1363 and 1550 cm^{-1} assigned to different types of oxycarbonates[1]. These bands were not seen in the $Rh(0.6)/La_2O_3(27)\cdot SiO_2$ catalyst.

Note the presence of two bands at 2500 and 2870 cm^{-1}. The band at 2870 cm^{-1} has been attributed to either formate or oxycarbonate overtones [1]. Similarly, the 2500 cm^{-1} signal could be attributed to a carbonate overtone [15]. Note, that the bands grow together with time on stream [5] and when He is fed at 673 K after reaction, these signals do not disappear. These bands might be related to the $Rh(0.6)/La_2O_3$ deactivation. The formate could be formed on the catalyst surface due to the interaction of adsorbed CO with surface OH. This mechanism was proposed on Ni/La_2O_3 by Verykios[21] in the presence of water vapor. For a more detailed analysis of these spectra see [5].

3.2.2. Effect of an inert gas and O_2 upon the regeneration of deactivated catalysts

If strongly adsorbed formate type species or carbonates formed during reaction block the active sites and progressively deactivate the catalyst, their elimination should restore the catalytic activity. To verify this hypothesis, the reduced catalyst was exposed to the reacting mixture (9% CO, 27% H_2O, 64% Ar ($H_2O/CO = 3:1$)) at 673 K during 20 h. Afterwards, air was fed for a period of 60 min at the same temperature. Then, the catalyst was reduced and the reacting mixture was fed again to observe the effect of the oxygen treatment upon the reaction rate.

In the first part of Fig. 4a, it is observed that when the reactant stream is restored after flowing Ar for 24 h at 673 K, the catalytic activity remains the same. This indicates that the deactivating compounds formed during reaction are not removed by the inert gas.

In the second part, Fig. 4a shows that after oxidation in air at 673 K and subsequent reduction, the catalyst activity was recovered reaching 92% of the initial value. After that, the solid deactivated progressively on stream following a similar trend to that of the previous run.

A similar experiment was carried out using the DRIFTS technique. This DRIFTS experiment was designed to investigate the fate of the oxygenates after treating the used catalyst with either He or diluted O_2. The two lowest IR spectra (Fig. 4b) show that flowing He at 673 K does not affect the 2500/2870 cm^{-1} bands. However, these bands disappear after a 10 min exposure to diluted O_2.

Combining the results shown in Fig. 4a and b, it is concluded that the oxygen treatment burns the formate and/or carbonate species that would be blocking the active sites and which would be responsible for the progressive deactivation of the $Rh(0.6)/La_2O_3$ catalyst.

In brief, the different stability of Rh/La_2O_3 and $Rh/La_2Si_2O_7\cdot SiO_2$ is due to the different basicity of the supports. Note that the surface of the latter is made up of the disilicate and silica. In fact, no free La_2O_3 was detected in this formulation [7]. When the support

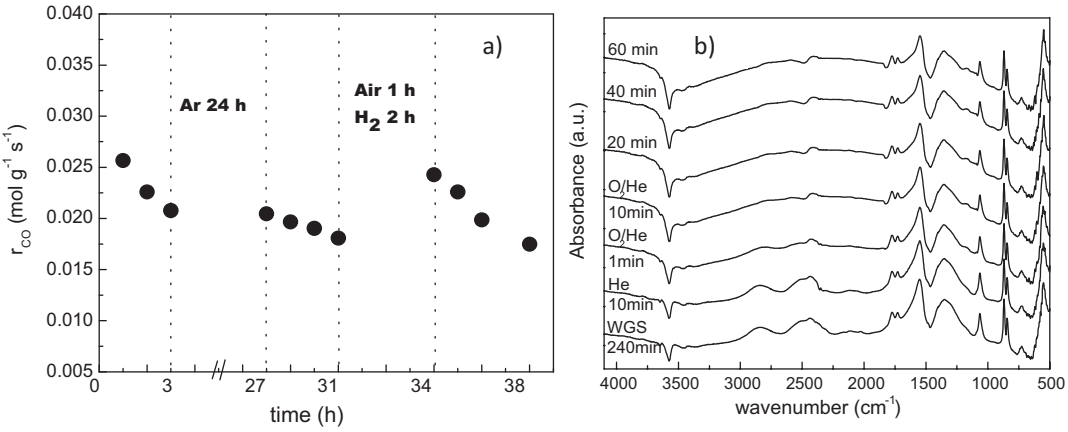

Fig. 4. (a) Effect of an inert and O_2(air) treatment over the Rh(0.6)/La_2O_3 catalyst activity. Reaction at 673K, feed 9% CO, 27% H_2O, 64% Ar. (b) DRIFTS results after treatment with oxygen at 673 K, O_2(5%)/He. WGS feed composition: 1.1% H_2O, 1.1% CO, 98.8% He. Spectra referenced to the spectrum of the reduced catalyst prior to gas admission.

is too basic, as La_2O_3, the stability of the formates and carbonates significantly increases. The deposition of the oxigenates leads to a slow but steady deactivation of this solid and the activity is recovered when both the formates and the newly formed carbonates are burnt in diluted O_2 at 673 K.

3.2.3. Comparison of different noble metal supported catalysts

The Rh(0.6)/La_2O_3(27)·SiO_2 and the Pt(0.6)/La_2O_3(27)·SiO_2 catalysts were evaluated in a conventional fixed-bed reactor under space velocities similar to those used in the membrane reactor (GHSV = 6–24 × 10^3 ml g^{-1} h^{-1}). The reaction was carried out at 673 K and the feed stream gas mixture was made up of CO and H_2O (H_2O/CO = 3). Under these conditions the methanation reaction is favored.

Fig. 5 shows that the Pt(0.6)/La_2O_3(27)·SiO_2 catalyst is highly selective to the WGS reaction, while the Rh(0.6)/La_2O_3(27)·SiO_2 solid presents a significant selectivity to methane. At the lowest space velocity, the Pt(0.6)/La_2O_3(27)·SiO_2 catalyst shows a high selectivity to the WGSR (S_{WGS} = 99.8%) while the Rh(0.6)/La_2O_3(27)·SiO_2 solid does not (S_{WGS} = 82.1%). Due to the high activity of the Pt catalyst, the CO conversion is close to the equilibrium value for the whole range of space velocities, in agreement with the results reported by Bi et al. [22]. Also note that on the Rh formulation, the measured CO conversion is above the calculated equilibrium value for the single WGSR due to the simultaneous occurrence of the irreversible methanation reaction.

3.2.4. Stability tests

The stability of the Pt(0.6)/La_2O_3(27)·SiO_2 catalyst was evaluated in a conventional fixed-bed reactor in differential and integral modes. In differential mode, the test was performed at 673 K, 1 atm, H_2O/CO = 2–3, d_p = 20 μm and GHSV = F_{To}/W = 6.7 × 10^6 ml g^{-1} h^{-1}. This high space velocity was required to eliminate external mass transport limitations [4]. Pt(0.6)/La_2O_3(27)·SiO_2 was stable for at least 50 h on stream and the reaction rate values were 0.028 mol g^{-1} min^{-1} (H_2O/CO = 3) and 0.018 mol g^{-1} min^{-1} (H_2O/CO = 2) (Vide infra).

Fig. 6 shows the stability test of the Pt catalyst under different WGS conditions (H_2O/CO = 1–3) at 673 K, 100 kPa and integral regime. The catalyst resulted stable at the different feed compositions (H_2O/CO = 1–3). Between shut-down and start-up cycles, the catalyst was exposed to an inert stream (Ar) at either 673 K or 298 K. The results show that the catalytic activity of the Pt catalyst is not affected by these cycles. Note that the catalytic measurements using a conventional reactor to study catalyst stability were made at conversions of ca. 50% (Fig. 6). Only the Fig. 5 that represents the effect of W/F on methane selectivity was recorded at conversions

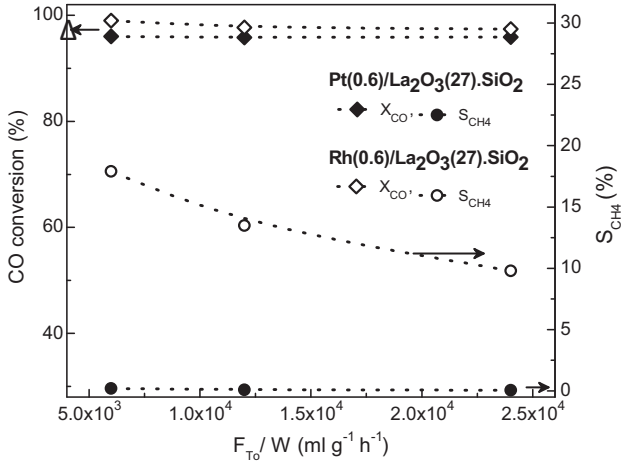

Fig. 5. Effect of the space velocity upon the CO conversion and CH_4 selectivity (S_{CH4}) in the conventional reactor. T = 673 K, P = 1 atm and H_2O/CO = 3 (equilibrium CO conversion = 96.2% (Δ)).
Reprinted from Cornaglia et al. [6], Copyright (2013), with permission from Elsevier.

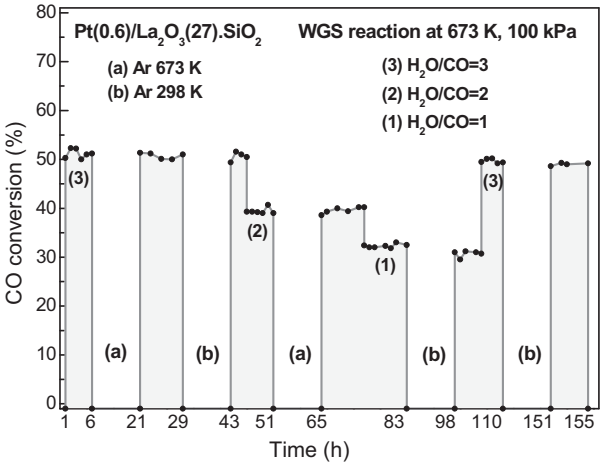

Fig. 6. *Stability test*. CO conversion vs time including start-up and shut-down cycles of the WGS reaction over the Pt(0.6)/La_2O_3(27)·SiO_2 catalyst at 673 K, 100 kPa, H_2O/CO = 1–3, GHSV = 1.2–1.5 × 10^6 h^{-1}.
Reprinted from Cornaglia et al. [7], Copyright (2013), with permission from Elsevier.

close to 100%. This high conversion level was chosen to enhance the possible formation of methane.

In the future a more comprehensive test of deactivation of this catalyst under different operating conditions will be carried out, e.g. WGS reaction and shutdowns using feed streams similar to those obtained from steam reformers fed either natural gas or ethanol.

Before using this solid in a membrane reactor, it is worthwhile to model the system to allow the previous simulation of the reactor behavior.

4. Mathematical model

A heterogeneous 1-D model was selected to represent the steady state operation of the laboratory membrane reactor. Under these conditions, the modeling of MRs presents interesting challenges because of the coupling of H_2 selective diffusion through the membrane with chemical reaction and mass transfer at the gas-solid interface.

The following assumptions were made: isobaric and isothermal conditions; axial dispersion phenomena were neglected; temperature and composition gradients in the radial coordinate were also neglected. Some reports consider that the catalyst layer is an infinitely thin layer [23]; however, in practice this is not true. Note that unlike all previous modeling studies about WGSR in membrane reactors [9], in this work the gas-solid mass transfer resistances were taken into account. Due to the non-porous nature of the catalyst support, the internal mass transfer resistances were neglected. Only H_2 permeated (100% selectivity).

Detailed information about the model is provided in the contribution dedicated to the heterogeneous modelling of the WGS reaction in a membrane reactor [6].

4.1. Mathematical model applied to $Pt(0.6)La_2O_3(27)\cdot SiO_2$

4.1.1. Reaction kinetics

Numerous studies concerning WGS reaction kinetics have been reported in the literature. It is generally accepted that the WGS proceeds via either a Langmuir–Hinshelwood (L.H.) mechanism, a redox mechanism, or an Eley–Rideal type mechanism. Depending on the mechanism and the rate limiting step, the reaction rate expressions have different dependences on the partial pressures of the compounds participating in the reaction.

The kinetic equation for the reactor modelling was derived through a modification of the Langmuir-Hinshelwood rate equation which was obtained for the $Rh(0.6)/La_2O_3(27)\cdot SiO_2$ formulation operating the reactor under differential mode [4]:

$$-r_{CO} = \frac{kK_{CO}K_{H_2O}P_{CO}P_{H_2O}}{\left(1 + K_{CO}P_{CO} + K_{H_2O}P_{H_2O}\right)^2} \quad (1)$$

It was also experimentally verified [4] that the addition of CO_2 in the reactant feed stream did not affect the reaction rate. However, when H_2 was added a negative reaction order for this reaction product was obtained.

The H_2 inhibition effect has been observed by many researchers when noble metals act as the active element and H_2 is a reaction product, e.g. Kalamaras et al. [24] reported for Pt (0.5 wt%)/TiO_2 the following reactions orders: $p_{CO}^{0.5}$, $p_{H_2O}^{1.0}$, $p_{H_2}^{-0.7}$, $p_{CO_2}^{0.0}$. These values are similar two those obtained for $Pt(0.6)/La_2O_3(27)\cdot SiO_2$ (Eq. (2)).

The only way that H_2 can negatively affect the reaction rate in this system is through competition for the same active sites with the reactants. If the H_2 would be adsorbed on different sites there should be no effect upon the reaction rate.

Table 2
Kinetic parameters used in the reactor model. Reprinted from Cornaglia et al. [6], Copyright (2013), with permission from Elsevier.

k	$1.39 \times 10^{13} e^{(-18600/T)}$	$mol_{CO}\ kg_{cat}^{-1}\ s^{-1}$
K_{CO}	$6.85 \times 10^{-12} e^{(15540/T)}$	kPa^{-1}
K_{H_2O}	$1.83 \times 10^{-9} e^{(10850/T)}$	kPa^{-1}
K_{H_2}	$4.25 \times 10^{-7} e^{(9334/T)}$	kPa^{-1}

In view of these facts and taking into account the reaction reversibility under integral regime, the rate equation resulted:

$$-r_{CO} = \frac{kK_{CO}K_{H_2O}P_{CO}P_{H_2O}}{\left(1 + K_{CO}P_{CO} + K_{H_2O}P_{H_2O} + \sqrt{K_{H_2}P_{H_2}}\right)^2}\left(1 - \frac{P_{H_2}P_{CO_2}}{P_{H_2O}P_{CO}K}\right) \quad (2)$$

Note that a corrective term was included in the numerator of Eq. (2) to account for the effect of the reverse WGSR. A new term was also added in the denominator to consider the strong adsorption of H_2, which is not negligible under integral mode.

This approach could be justified because the Pt and Rh noble metals have a similar catalytic behavior. Besides, both catalysts were prepared in the same way with the same support ($La_2Si_2O_7\cdot SiO_2$) and employing an identical load of noble metal (0.6 wt%).

The numerical values of the adsorption constants (Ki) and the surface reaction rate (ki) were calculated from the reaction rate data obtained for the platinum containing catalyst (Table 2).

4.2. Comparison between model and experimental data

This comparison was made on the basis of the effect of space velocity and particle size on the MR performance.

4.2.1. Effect of the space velocity

Fig. 7a shows the effect of the space velocity on the CO conversion and H_2 recovery. The latter parameter, which indicates the fraction of H_2 recovered in the permeate side of the membrane reactor, is defined as follows:

$$R_{H_2}(\%) = \frac{H_{2,P}}{H_{2,P} + H_{2,R}} \times 100 \quad (3)$$

where $H_{2,P}$ and $H_{2,R}$ correspond to the hydrogen flow rate ($N\,mL\,min^{-1}$) in the permeate and the retentate side, respectively.

In the figure the experimental data are indicated by symbols and the model predictions, obtained by using the heterogeneous model, are indicated by lines. As expected, the CO conversion shows a decline with increasing GHSV as a result of the shortening of the contact time of the syngas with the catalyst surface. Besides, a reduction in hydrogen recovery is also observed with increasing feed flow rate. In particular, the lower contact times cause the H_2 recovery to drop from 81% to 31%, for a total increase in the gas flow rate close to 4 times. In line with the decrease of the H_2 recovery, such a behavior is consistent with the idea that by increasing the feed flow rate, the relative importance of the mass transfer resistance in the composite membrane itself becomes more relevant. Another reason that may be connected with the CO conversion drop is that the reactants residence time decreases. However, due to the high activity of the Pt catalyst, the conversion drop is not so severe as that corresponding to the H_2 recovery.

4.2.2. Analysis of the influence of particle diameter (d_p) on MR performance

The influence of the particle diameter on the performance of the MR is analyzed in order to test the validity of the model. The effect of the space velocity on the CO conversion and H_2 recovery is shown for $d_p = 20\ \mu m$ and for $d_p = 230\ \mu m$ (Fig. 7a and b).

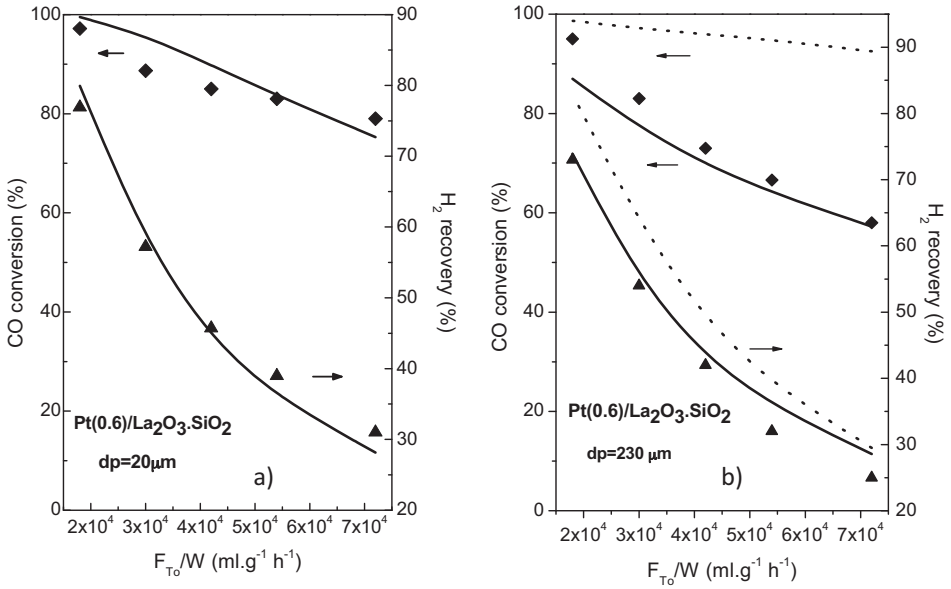

Fig. 7. Effect of the space velocity (F_{To}/W) on the CO conversion and H_2 recovery using the Pt(0.6)/La_2O_3(27)·SiO_2. (a) d_p (20 μm) and (b) d_p (200 μm) . T = 673 K, P = 1 atm, H_2O/CO = 2 and F_{SG} = 200 N ml min^{-1}.
Reprinted from Cornaglia et al. [6], Copyright (2013), with permission from Elsevier.

Note that with both particle sizes, the heterogeneous mathematical model satisfactorily reproduces the experimental tendencies. The comparison between Fig. 7a and b reflects that at lower d_p, the CO conversion and H_2 recovery are higher in comparison with the results obtained using a larger particle size. As the d_p increases, the external particle surface area per unit reactor volume decreases and the external mass transfer limitations may become more important and, consequently, the conversion levels significantly decrease. This fact confirms that the external mass transfer limitations in the membrane reactor cannot be neglected. Simulations by means of a pseudohomogeneous model were also performed, setting very high values of the mass transfer coefficients in the present model. In this case, the CO conversions (dottted lines in Fig. 7b) and H_2 recoveries were overestimated and it was not possible to reproduce the effect of the particle size experimentally observed on the reactor performance.

Regarding the H_2 recovery, it also decreases with respect to that of smaller particles (compare Fig. 7a and b). This phenomenon is associated with lower driving forces through the membrane for the case d_p = 230 μm, due to both the lower CO conversions (less H_2 is being generated) and the higher interfacial gradients, i.e., the bulk H_2 partial pressures become considerably lower than their values on the catalyst surface.

The results shown in Fig. 7 confirm the necessity of using a heterogeneous model to simulate the reactor behavior in the range of operating conditions explored.

Experimentally we did not notice a significant pressure drop in our membrane reactor when changing the particle size from 230 μm to 20 μm. This is why we did not attempt to calculate the pressure drops using the two different particle sizes.

5. Pd-membrane reactor high-pressure tests

In order to assess the performance of the Pt(0.6)/La_2O_3(27)·SiO_2 catalyst in the membrane reactor, different runs were performed between 673 and 723 K, with the pressure ranging from 100 kPa to 800 kPa, feed molar ratio H_2O/CO = 2 and space velocities of GHSV = 3120, 6240 and 9360 h^{-1} in the retentate side [7].

The temperature limits were imposed by two factors: (i) T < 673 K increases the CO poisoning of the membrane that reduces the hydrogen permeability, (ii) T > 723 K shortens the membrane durability because it overtakes the upper operating temperature at which occur pinhole and cracks of the Pd-Ag alloy.

The performance of the membrane reactor was evaluated in first approximation in terms of the CO conversion, CH_4 selectivity and hydrogen recovery (R_{H2}).

Effect of space velocity (GHSV) and pressure. Fig. 8 shows the CO conversion and H_2 recovery as a function of the feed (retentate) pressure for three different space velocities (3120, 6240 and 9360 h^{-1}). The pressure increases the hydrogen permeation through the membrane. Therefore, the hydrogen removal through the membrane promotes the CO conversion through the "shift effect". However, the significant drop in H_2 recovery is due to the decrease of the reactants residence time. Note that an increasing retentate pressure beyond 800 kPa will produce only a small increment in H_2 recovery and almost no effect in CO conversion. Therefore, it is concluded that using this membrane type is not effective to increase the pressure beyond 800 kPa. Fig. 8 also shows a positive temperature effect. This is mainly due to the fact that a higher temperature increases both the WGS reaction rate and, to a smaller extent, the H_2 permeation through the membrane.

CH_4 selectivity. The values obtained in the membrane reactor at 6240 h^{-1} with a sweep gas flow rate of 500 N mL min^{-1} are 100 times smaller than the theoretical values calculated under thermodynamic equilibrium conditions [7]. Accordingly, these membrane reactor tests further verify that the Pt(0.6)/La_2O_3(27)·SiO_2 catalyst does not promote methane formation.

5.1. Comparison with published data

A comprehensive comparison between our results and those reported in the literature is not easy because of the different operating conditions (wide variety of membrane characteristics, reactor configurations and experimental conditions). Particularly important is the operation pressure since the difference between retentate and permeate pressures constitutes the driving force for the permeation process and, consequently, governs the H_2 permeation flux and the CO conversion. In order to maximize the pressure difference several authors introduce a sweep gas in the system [7,25,27,28].

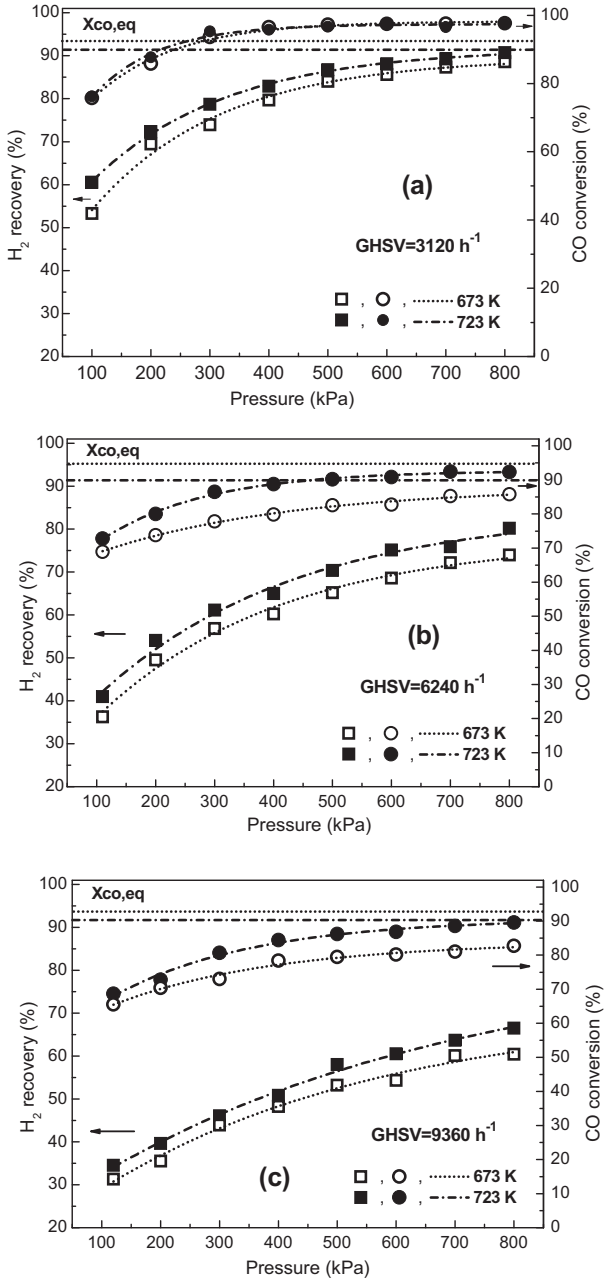

Fig. 8. Effect of pressure and temperature upon the CO conversion and H_2 recovery ($H_2O/CO = 2$) using the $Pt(0.6)/La_2O_3(27)\cdot SiO_2$, at different space velocities, F_{SG} = 500 N mL min^{-1}(Wcatalyst = 1.5 g).
Reprinted from Cornaglia et al. [7], Copyright (2013), with permission from Elsevier.

In a more comprehensive evaluation of WGS membrane reactors additional factors should be considered such as H_2 purity, H_2 production ($Nm^3\ m^{-2}\ h^{-1}$) and stability (Table 3).

Our membrane is by far more stable than composite membranes but the permeability ratio is inverted. As previously mentioned, working under integral conditions (membrane reactor) increases the probability that the methanation reaction occurs. In our case, for catalysts based on Pt, it was previously shown that no formation of methane occurred under these conditions. However, in most publications, methane formation is ignored.

Caution should be exercised when analyzing literature data because those experiments run at $T < 673$ K could include the negative effect of CO adsorption on the membrane upon H_2 permeance.

Table 3
Comparison of WGS membrane reactors performance. Reprinted from Cornaglia et al. [7], Copyright (2013), with permission from Elsevier.

Membrane	δ[a] (μm)	Catalyst	$T_{reaction}$ (K)	$P_{reaction}$ (kPa)	H_2O/CO (molar)	GHSV (h^{-1})	H_2 prod. flux ($Nm^3\ m^{-2}\ h^{-1}$)	X_{CO}[b] (%)	H_2 Rec[c] (%)	H_2 purity (%)	Ref. #
Pd-Ag[d]	150	$Pt/La_2O_3\cdot SiO_2$	673	800	2	3120	0.55	97.5	88	99.999	
			723	800	2	3120		97.7	90	99.999	
			673	800	2	6240		85.8	75.1	99.999	
			723	800	2	6240		92.3	85.4	99.999	
							0.62				Our work [7]
							0.96				
							1.2				
Pd/PSS	29	Fe_3O_4/Cr_2O_3[e]	683	600	3.6	1003	2.97	85.0	82.0	97.0	[25]
Pd/PSS	20	Fe_3O_4/Cr_2O_3[e]	663	1100	3	3450	–	85	66	95	[26]
Pd-Ag/Pinconel	8.8	Fe_3O_4/Cr_2O_3[e]	723	1440	1.6	5502	9.74	93.6	78.1	99.9[f]	[27]
Pd/PSS	8.3	Fe_3O_4/Cr_2O_3[e]	713	2000	2.5	5650	11.67	84.9	42.8	99.5	[28]
Pd/CS[g]	1.4	$Pt/Ce_{0.6}Zr_{0.4}O_2$	623	1200	2.9	14100	27.95	94.9	48.7	99.7	[22]

[a] Pd or Pd-Ag thickness.
[b] CO conversion.
[c] H_2 recovery.
[d] Self standing.
[e] Commercial formulations.
[f] Estimated from ideal selectivity data provided in reference [27].
[g] Ceramic support (CS).

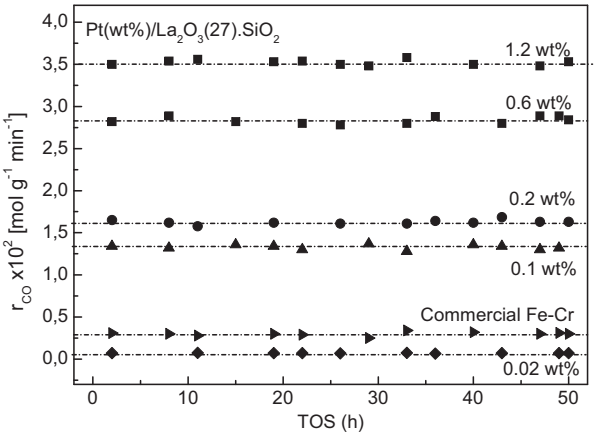

Fig. 9. Stability tests of catalysts at 673 K, 1 bar, $H_2O/CO = 3$. GHSV = 2.8×10^6 h^{-1} (Pt catalysts) and GHSV = 7.84×10^6 h^{-1} (Commercial Fe-Cr formulation).
Reprinted from Cornaglia et al. [8], Copyright (2014), with permission from Elsevier.

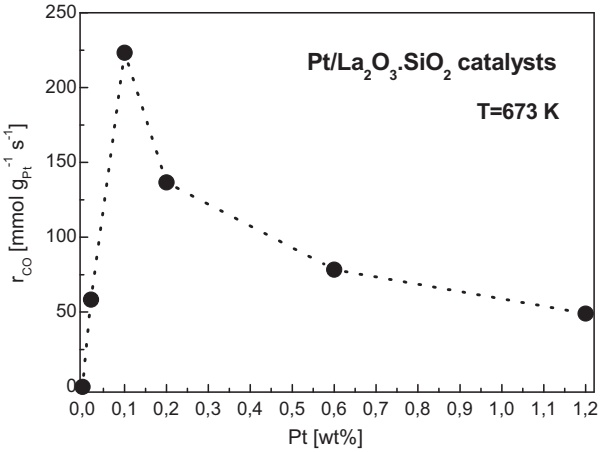

Fig. 10. Effect of weight percent of Pt over the catalytic activity at 673 K, 100 kPa, $H_2O/CO = 3$ and GHSV = 2.8×10^6 h^{-1}.
Reprinted from Cornaglia et al. [8], Copyright (2014), with permission from Elsevier.

Concerning H_2 recoveries, note that the values are generally lower with composite membranes with the aggravating factor that in the latter case the H_2 permeated does not reach the purity required to feed PEM fuel cells. In previous works [7,8], operating with a pressure difference of 800 kPa and a sweep gas flow rate of 500 ml/min, hydrogen recoveries between 88 and 90% were reported. The H_2 production flux is another key parameter and, as expected, it increases sharply for composites due not only to the thinner metal layers but also to the existence or development during use of pinholes and/or cracks in the alloy film. This, in turn, negatively affects the H_2 purity.

6. Optimal Pt load of a Pt(wt%)/La_2O_3·SiO_2 WGS catalyst

To optimize the content of platinum in the Pt(wt%)/La_2O_3(27%)·SiO_2 catalysts, activity, stability and selectivity were measured with varying Pt loads (wt% = 0.02, 0.1, 0.2, 0.6 and 1.2). The reaction rates were obtained at 673 K, 100 kPa and $H_2O/CO = 3$ using the conventional catalytic fixed-bed tubular reactor in differential mode ($X_{CO} < 10\%$). To avoid internal and external mass transport limitations, the kinetic measurements were carried out at high flow rates (744 NmL min^{-1}) and with small particle sizes ($d_p < 20\ \mu m$) in order to avoid mass transfer limitations. The first gas sample was taken 30 minutes after switching on the reactant stream.

Fig. 9 shows that all the catalysts were stable for at least 50 h on stream. They did not form carbon and they were 100% selective to the WGS reaction. The Pt(0.1–1.2) catalysts showed higher catalytic activities than a commercial one. The catalysts with 0.6 (Fig. 6) and 0.1 wt% of platinum were also stable under WGS conditions in integral mode. Expressing the reaction rate values per gram of platinum (Fig. 10), a maximum is seen for the solid with 0.1 wt % of noble metal. This particular point and the one pertaining to 0.6 wt% were checked at least 25 times using many different batches.

In order to verify whether all catalysts (with wt% of Pt = 0.02 through 1.2) presented a similar structure, they were characterized using XRD, laser Raman and BET.

All the solids presented a very low crystallinity disilicate ($La_2Si_2O_7$) and amorphous SiO_2 phases, similarly to the finding reported by Vidal et al. [29]. All of them presented similar phases and no reflections corresponding to Pt° ($2\theta = 40.7°$ and 46.3°) were observed, possibly due to the low noble metal loading and/or small Pt crystallite size of these formulations (Fig. 11).

It is important to mention that the La_2O_3·SiO_2 support did not present Raman active bands [7]. Furthermore, the Raman spectra of the used Pt(wt%)/La_2O_3(27)·SiO_2 catalysts did not show bands corresponding to the presence of either carbonates or graphitic residues. Remember that this spectroscopic tool is very sensitive to the presence of graphitic residues. BET surface areas of approximately 180 m^2 g^{-1} and bulk densities of 0.5 g mL^{-1} were measured for all catalysts.

In brief, with the characterization techniques employed, no structural differences were observed for the different Pt(wt%)/La_2O_3·SiO_2 solids (with wt% = 0.02–1.2 wt%).

Binding energies and atomic surface ratios of fresh and used catalysts are reported in Table 4. For the Pt(0.1) catalyst, the Pt $4f_{7/2}$ binding energy at 70.8 eV indicates that all the platinum was present as Pt°, remaining unchanged after exposure to the WGS reaction stream. Also, the XPS intensity ratios of La 3d5/2/Si 2s, Pt 4f 7/2/Si 2s and O 1s/Si 2s were not modified. This is consistent with the stability of this catalyst under reaction conditions (Fig. 9).

The fresh-reduced and the used Pt(0.6)/La_2O_3·SiO_2 catalyst presents a signal at 70.8 eV corresponding to metallic platinum but a second Pt component is observed at 71.6 eV corresponding to an oxidized species. This signal could be assigned to $Pt^{\delta+}$ species [30,31] which could arise from incomplete precursor decomposition.

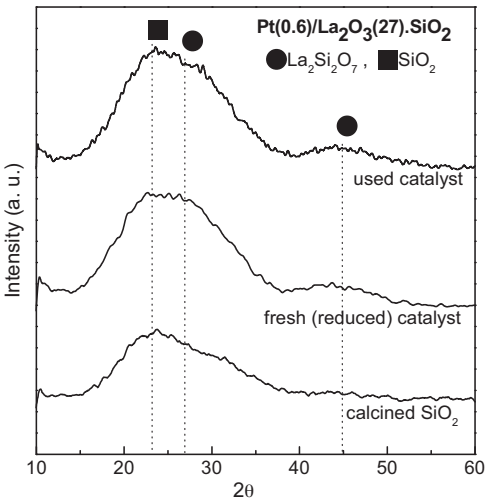

Fig. 11. XRD patterns for the fresh and used Pt(0.6)/La_2O_3·SiO_2 catalysts (after being on stream at $T = 673$ K, $P = 1$ atm and $H_2O/CO = 3$).
Reprinted from C.A. Cornaglia et al. [6], Copyright (2013), with permission from Elsevier.

Table 4
XPS data of fresh (reduced) and used (after WGS reaction) Pt(wt%)/La_2O_3·SiO_2 catalysts. Reprinted from Cornaglia et al. [8], Copyright (2014), with permission from Elsevier.

Solids	Treatment	Binding energies (eV)[a]				Surface atomic ratios		
		La $3d_{5/2}$	O 1s	Si 2s	Pt $4f_{7/2}$	La $3d_{5/2}$ /Si 2s	Pt $4f_{7/2}$ /La 3d	O 1s /Si 2s
Pt(0.1)/ La_2O_3·SiO_2	Reduced [c]	836.3	532.8	154.3	70.8	0.08	0.007	1.7
	Used in WGSR[d]	836.6	533.1	154.3	70.8	0.07	0.008	1.7
Pt(0.6)/ La_2O_3·SiO_2	Reduced [c]	835.4	532.5	154.3	70.8 (38)[b] 71.6 (62)[b]	0.07	0.03	1.7
	Used in WGSR[d]	835.3	532.3	154.3	70.9 (52)[b] 71.7 (48)[b]	0.06	0.04	1.8
Pt(1.2)/ La_2O_3·SiO_2	Reduced [c]	835.4	532.6	154.3	70.9 (34)[b] 71.5 (66)[b]	0.06	0.11	1.6
	Used in WGSR[d]	835.3	532.5	154.3	70.8 (68)[b] 71.8 (32)[b]	0.07	0.09	1.7

[a] Referenced to the signal of Si 2s at 154.3 eV.
[b] The relative percent of platinum species is given in parentheses.
[c] Reduced at 673 K under flowing hydrogen during 2 h.
[d] After 50 h on stream at 673 K and $H_2O/CO = 3$.

Reduced and used Pt(1.2)/La_2O_3·SiO_2 solids also show components at binding energies corresponding to Pt° and $Pt^{\delta+}$ species, similar to the signals observed on the Pt(0.6)/La_2O_3·SiO_2 catalyst (Table 4). The solids with 0.6 and 1.2 wt% of Pt do not present significant changes in the XPS intensity ratios of La $3d_{5/2}$/Si 2s, Pt $4f_{7/2}$/Si 2s and O1s/Si 2s (Table 4).

For the Pt(0.6) and Pt(1.2) formulations, the surface Pt $4f_{7/2}$/Si 2s ratio was practically the same before and after catalyzing the WGS reaction, and this could indicate that the surface Pt concentration remains practically unchanged.

6.1. Thermal evolution of Pt precursors

For similar Pt precursors such as $[Pt^{II}(NH_4)_2]Cl_4$, $[Pt^{IV}(NH_4)_2]Cl_6$, $[Pt^{II}(NH_3)_4](NO_3)_2$ [32], the final decomposition temperatures are between 523 and 623 K, depending upon the gas atmosphere (air or hydrogen). Goguet et al. [33], for a Pt/SiO_2 catalyst, reported a maximum Pt precursor decomposition temperature of 613K under Argon. By EXAFS, they observed a consequent formation of PtO species (main phase) and Pt° species, using $Pt(NH_3)_4(OH)_2$·xH_2O as precursor.

Kinoshita et al. [34] reported similar thermograms of $Pt(NH_3)_4Cl_2$·$0.3H_2O$ in argon and air, giving evidence of an intermediate product in the weight-loss curve. Wendlandt et al. [35] observed the evolution of NH_3 in air from the anhydrous compound $Pt(NH_3)_4Cl_2$ to form trans-$Pt(NH_3)_2Cl_2$. Then, at approximately 593–623 K, decomposition to metallic platinum was observed. The authors concluded (based on weight-loss measurements) that the thermal stability of $Pt(NH_3)_4Cl_2$·$0.3H_2O$ is higher than that of $Pt(NH_3)_4(OH)_2$.

Richard et al. [36] observed two endothermic thermal events for the $Pt(NH_3)_4Cl_2$ precursor by TG/DTG/DTA/MS. The first event occurred from 548 to 588 K and involved the loss of two moles of ammonia (detected by mass spectrometry) to form the intermediate $Pt(NH_3)_2Cl_2$ compound. The subsequent decomposition to metallic platinum occurred from 588 to 643 K also forming N_2, NH_3 and HCl. By MS, the authors concluded that the decomposition of diamineplatinum (II) chloride does not lead to the formation of a stable $PtCl_2$. A similar conclusion was reported by Hernández et al. [37] who did not propose the formation of PtClx species, either. If the PlClx species were formed during the $Pt(NH_3)_4Cl_2.H_2O$ decomposition, they could decompose at ca. 753 to 763 K under helium or oxygen to form metallic platinum and Cl_2. Radivojevic et al. [32] reported a decomposition temperature of $PtCl_4$ under oxygen from 553 to 623 K to form $PtCl_2$. They also reported the subsequent decomposition to form Pt and Cl_2 from 623 to 803 K.

The formation of PtO [33], $Pt(NH_3)_2Cl_2$ [34–36] or PtClx, in addition to Pt° as decomposition products could be consistent with the presence of $Pt^{\delta+}$ and Pt° observed by XPS for the catalysts with 0.6 and 1.2 wt% of Pt.

Due to the differences observed by XPS concerning the Pt oxidation states, the high activity (per gram of noble metal) of the Pt(0.1) solid could be due to the exclusive presence of Pt°.

From this rapid literature revision, it is concluded that the interaction of the noble metal precursor with the support greatly depends on several factors such as the nature of the support, the structure of the metal complex and the nature of the gaseous atmosphere. In this way, the existence of partially reduced Pt species can be expected. A more thorough study is needed to fully elucidate the redox behavior of platinum supported on the La_2O_3·SiO_2 solid.

6.2. Reduction temperature effect

To verify the negative effect of the Pt oxidized species on the specific catalytic activity, tests were carried out reducing the solids at higher temperature (773 K). It was shown [8] that higher reduction temperatures allow higher specific activity values for the catalysts with 0.6 and 1.2 wt% of Pt, increasing the presence of metallic platinum species (Pt°). However, higher reduction temperatures favor the noble metal sintering, not allowing the achievement of the catalyst specific activity observed with 0.1 wt% of platinum.

Thus, the Pt/La_2O_3·SiO_2 solid with 0.1 wt% of Pt is the most efficient, stable, selective to the WGSR and no-carbon forming catalyst. For this reason, this formulation was selected to be used in a membrane reactor.

6.3. Membrane reactor WGS reaction tests

Prior to testing the Pt(0.1)/$La_2O_3(27)$·SiO_2 catalyst in the membrane reactor, a stability test in integral mode and including several start-ups and shut-downs was carried out (similar to the previous stability test carried out for the Pt(0.6) catalyst (Fig. 6)). This test was carried out in the conventional fixed-bed tubular reactor including several start-ups and shut-downs of the reaction system at 673 K, 100 kPa and under different WGS conditions ($H_2O/CO = 1–3$, GHSV = $1.2–1.5 \times 10^6\ h^{-1}$).

The catalyst was stable under the different WGS feed compositions ($H_2O/CO = 1–3$). Between shut-down and start-up cycles, the

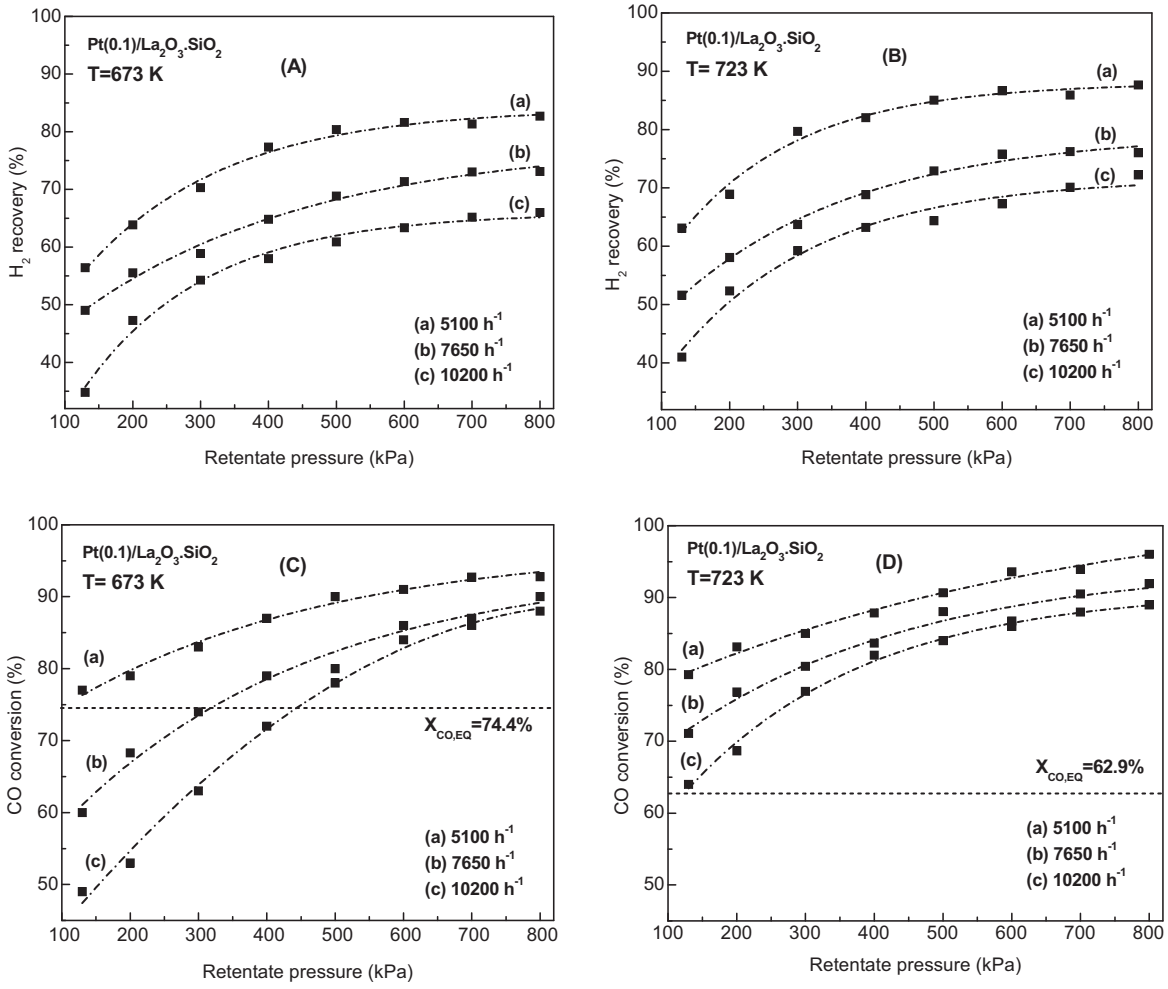

Fig. 12. Effect of the retentate pressure upon the CO conversion and the H_2 recovery at 673 K (A and C) and 723 K (B and D) at different space velocities (5100, 7650 and 10200 h^{-1}). Feed stream composition: 40% H_2, 40% H_2O, 12% CO_2, 8% CO; F_{SG} = 500 N mL min^{-1}.
Reprinted from Cornaglia et al. [8], Copyright (2014), with permission from Elsevier.

catalyst was exposed to flowing Ar at either 673 K or 298 K. The results show that the stability of the Pt catalyst was not affected by these cycles. It is important to mention that in this experiment, no methane was detected.

To study the behavior of the Pt(0.1)/La_2O_3·SiO_2 catalyst in the membrane reactor, several runs were performed between 673 and 723 K, with the retentate pressure ranging from 130 kPa to 800 kPa, feed stream with a reformer outlet type molar composition (40% H_2O, 40% H_2, 12% CO_2, 8% CO), a sweep gas flow rate of 500 N mL min^{-1} and space velocities of GHSV = 5100, 7650 and 10,200 h^{-1}. Remember that the Pd-Ag membrane does not catalyze the WGS reaction [7].

Fig. 12 shows the CO conversion and H_2 recovery at 673 and 723 K, as a function of the feed pressure (retentate) at different space velocities. The pressure difference increases the hydrogen permeation through the membrane. Therefore, the hydrogen removal promotes the CO conversion, reaching values higher than the equilibrium ones (conventional reactor) shown in Fig. 12c and d.

A significant drop in H_2 recovery occurs when the space velocity increases (Figs. 12 A and B). This effect is due to the decrease of the reactants residence time in the reactor. At feed pressures, values between 600 and 800 kPa, the H_2 recovery varies slightly, while the effect upon the CO conversion is more significant. Therefore, a higher CO conversion could be obtained operating at pressures higher than 800 kPa. However, the CO conversion values at 800 kPa slightly varied between 673 K and 723 K. The best catalyst-membrane reactor performance was obtained at 800 kPa, 723 K and at a space velocity of 5100 h^{-1}, allowing a CO conversion value of 96% with a H_2 recovery of 88%.

Comparing Fig. 12A and C at 673 K with Fig. 12B and D at 723 K, a positive temperature effect is observed. This is mainly due to the fact that a higher temperature increases the WGS reaction rate and to a smaller extent the H_2 permeation through the membrane. It is important to mention that in these membrane reaction tests, a maximum CH_4 selectivity value of 0.1% was measured despite the presence of H_2 from the inlet.

Table 5 shows a comparison of several Pd-membrane reactor performances from the literature and from this work obtained feeding streams with compositions similar to typical reforming outlets. Since the data reported were obtained under different operating conditions, it is difficult to reach useful conclusions without a deeper data analysis.

First of all, note that the feed compositions are similar. Then, temperature, pressure, and space velocity are the most important variables to consider. Therefore, in order to compare performances, one has to consider the data obtained with the closest values of these variables. With this in mind, and concentrating on the underlined data of Table 5, it is observed that the three underlined temperatures of our data are within 20 K, and our formulation is in between the other two.

Table 5
Comparison of WGS Pd-membrane reactors performances from the literature feeding streams with compositions similar to typical reforming outlets. Reprinted from Cornaglia et al. [8], Copyright (2014), with permission from Elsevier.

Membrane	Catalyst	T (K)	P (kPa)	Feed composition $H_2O/CO/H_2/CO_2/CH_4$	GHSV (h^{-1})	X_{CO}[d] (%)	Rec H_2[e] (%)	$\alpha_{H2/N2}$[f]	Ref
CER-Pd (1.4 μm)[a]	$Pt(1\%)/Ce_{0.6}Zr_{0.4}O_2$	623	400–1200	34.4/11.8/45.3/7.4/1.1	4050	86–95.5	41–89	> 5000	[22]
PSS-Pd (29 μm)[b]	Fe-Cr oxide	683	100–600	27.1/7.6/45.8/26.4/0	1394	58–85	28–80	310–90	[25]
PSS-Pd (20 μm)[b]	Fe-Cr oxide	663	1100	32/8/36/24/0	3450	77	70	303–173	[26]
Pd-Ag (150 μm)[c]	$Pt(0.1\%)/La_2O_3{\cdot}SiO_2$	673	100–800	40/8/40/12/0	5100	77–92.5	55–82	∞	
					10,200	49–87	35–65		Our work [8]
		723	100–800	40/8/40/12/0	5100	80–96	62–88	∞	
					10,200	64–89	40–70		

[a] CER (ceramic).
[b] PSS (porous stainless).
[c] (Self-supported) membrane.
[d] CO conversion.
[e] H_2 recovery.
[f] Permeation selectivity.

The pressure varies more but again, it is in between the extreme values and the same reasoning applies. Our GHSV is the highest and this parameter reduces both CO conversion and H_2 recovery. Therefore, our catalyst was assayed under the most unfavorable space velocity conditions. From this analysis, it is concluded that if the three formulations were assayed under identical conditions, it is highly probable that ours would be the best one.

7. Conclusions

Out of the three noble metal catalysts prepared with the same load the $Pt(0.6)/La_2O_3(27){\cdot}SiO_2$ resulted the most active, non-methane forming and the most stable one under WGS integral reaction conditions. Although the $Rh(0.6)/La_2O_3$ has a high initial activity it deactivates 53% during 50 hours on stream. It was shown that this was due to the irreversible adsorption of oxygenates. This formulation recovered its activity after burning the oxygenated residues. This behavior is consistent with the higher basicity of La_2O_3.

On a gram of Pt basis, the most active catalyst had a Pt load of 0.1%. XPS showed that on this catalyst the noble metal was completely reduced to Pt^0. This was not the case for catalysts with higher loads (up to 1.2%).

A heterogeneous 1-D model was selected to simulate the steady state operation of the membrane reactor. This is a requirement due to the high activity of the best catalysts developed in this study. To the best of our knowledge, nobody else has used a heterogeneous model to simulate the behavior of membrane reactors for WGSR.

Our membrane reactor equipped with our optimized catalyst ($Pt(0.1)/La_2O_3(27){\cdot}SiO_2$) shows one of the best performances reported in the literature.

Acknowledgements

The authors wish to acknowledge the valuable collaboration of Daniel Borio, Patricio Ruiz, Silvano Tosti and their teams. Also recognize the financial support received from UNL, CONICET and ANPCYT. Thanks are also given to ANPCyT for the purchase of the Raman instrument (PME 87-PAE 36985) and the UHV MultiAnalysis System (PME 8-2003) and to the Japan International Cooperation Agency (JICA) for the donation of the XRD instrument.

References

[1] S. Irusta, L.M. Cornaglia, E.A. Lombardo, J. Catal. 210 (2002) 7–16.
[2] S. Irusta, J. Munera, C. Carrara, E.A. Lombardo, L.M. Cornaglia, Appl. Catal. A: Gen. 287 (2005) 147–158.
[3] J.F. Múnera, C. Carrara, L.M. Cornaglia, E.A. Lombardo, Chem. Eng. J. 161 (2010) 204–211.
[4] C.A. Cornaglia, J.F. Múnera, E.A. Lombardo, Ind. Eng. Chem. Res. 50 (2011) 4381–4389.
[5] C.A. Cornaglia, J.F. Múnera, L.M. Cornaglia, E.A. Lombardo, P. Ruiz, A. Karelovic, Appl. Catal. A: Gen. 435–436 (2012) 99–106.
[6] C.A. Cornaglia, M.E. Adrover, J.F. Mùnera, M.N. Pedernera, D.O. Borio, E.A. Lombardo, Int. J. Hydrogen. Energy 38 (2013) 10485–10493.
[7] C.A. Cornaglia, S. Tosti, M. Sansovini, J. Múnera, E.A. Lombardo, Appl. Catal. A: Gen. 462–463 (2013) 278–286.
[8] C.A. Cornaglia, S. Tosti, J. Múnera, E.A. Lombardo, Appl. Catal. A: Gen. 486 (2014) 85–93.
[9] K. Babita, S. Sridhar, K.V. Raghavan, Int. J. Hydrogen Energy 36 (2011) 6671–6688.
[10] X. Liu, W. Reuttinger, X. Xu, R. Farrauto, Appl. Catal. B: Environ. 56 (2005) 69–75.
[11] C. Ratnasamy, J.P. Wagner, Catal. Rev. 51 (2009) 325–440.
[12] P. Panagiotopolou, D.I. Kondarides, Appl. Catal. B: Environ. 101 (2011) 738–746.
[13] C.I. Vignatti, M.S. Avila, C.R. Apesteguia, T.F. Garetto, Catal. Today 171 (2011) 297–303.
[14] L.M. Cornaglia, J. Munera, S. Irusta, E.A. Lombardo, Appl. Catal. A: Gen. 263 (2004) 91–101.
[15] B. Kingenberg, M. Vannice, Chem. Matter 8 (1996) 2755–2768.
[16] X. Wang, R.J. Gorte, J.P. Wagner, J. Catal. 212 (2002) 225–230.

[17] A. Goguet, R. Burch, Y. Chen, C. Hardacre, P. Hu, R.W. Joyner, F.C. Meunier, B.S. Mun, D. Thompsett, D. Tibiletti, J. Phys. Chem. C 111 (2007) 16927–16933.
[18] A. Goguet, F. Meunier, J.P. Breen, R. Burch, M.I. Petch, A. Faur Ghenciu, J. Catal. 226 (2004) 382–392.
[19] S. Hilaire, X. Wang, T. Luo, R.T. Gorte, J.P. Wagner, Appl. Catal. A: Gen. 215 (2001) 271–278.
[20] P. Panagiotopoulou, D.I. Kondarides, Catal. Today 112 (2006) 49–52.
[21] X.E. Verykios, Int. J. Hydrogen Energy 28 (2003) 1045–1063.
[22] Y. Bi, H. Xu, W. Li, A. Goldbach, Int. J. Hydrogen. Energy 34 (2009) 2965–2971.
[23] P. Boutikos, V. Nikolakis, J. Membrane Sci. 350 (2010) 378–386.
[24] C.M. Kalamaras, P. Panagiotopoulou, D.I. Kondarides, A.M. Efstathiou, J. Catal. 264 (2009) 117–129.
[25] P. Pinacci, M. Broglia, C. Valli, G. Capannelli, A. Comite, Catal. Today 156 (2010) 65–172.
[26] S. Liguori, P. Pinacci, P.K. Seelam, R. Keiski, F. Drago, V. Calabrò, A. Basile, A. Iulianelli, Catal. Today 193 (2012) 87–94.
[27] A.S. Augustine, Y.H. Ma, N.K. Kazantzis, Int. J. Hydrogen Energy 36 (2011) 5350–5360.
[28] J. Catalano, F. Guazzone, I. Mardilovich, N. Kazantzis, Y.H. Ma, Ind. Eng. Chem. Res. 52 (2013) 1042–1055.
[29] H. Vidal, S. Bernal, R. Baker, D. Finol, J.A. Perez, J.M. Pintado, J.M. Rodríguez-Izquierdo, J. Catal. 183 (1999) 53–62.
[30] E.A. Kozlova, T.P. Lyubina, M.A. Nasalevich, A.V. Vorontsov, A.V. Miller, V.V. Kaichev, V.N. Parmon, Catal. Commun. 12 (2011) 597–601.
[31] S. Kim, H.H. Lee, S.C. Hong, Appl. Catal. A: Gen. 423–424 (2012) 100–107.
[32] D. Radivojevic, K. Seshan, L. Lefferts, Appl. Catal. A: Gen. 301 (2006) 51–58.
[33] A. Goguet, D. Schweich, J.-P. Candy, J. Catal. 220 (2003) 280–290.
[34] K. Kinoshita, K. Routsis, S. Bett, Thermochim. Acta 10 (1974) 109–117.
[35] W.W. Wendlandt, Texas J. Sci. 14 (1962) 264.
[36] M.A. Richard, R.J. Pancirov, J. Therm. Anal. 32 (1987) 825–834.
[37] J.O. Hernández, E.A. Choren, Thermochim. Acta 71 (1983) 265–272.